Giant magnetocaloric effect driven by first-order magnetostructural transition in cosubstituted Ni-Mn-Sb Heusler compounds: Predictions from *ab initio* and Monte Carlo calculations

Sheuly Ghosh[*] and Subhradip Ghosh[†]

Department of Physics, Indian Institute of Technology Guwahati, Guwahati-781039, Assam, India

Using density functional theory and a thermodynamic model [V. Sokolovskiy *et al.* Phys. Rev. B **86**, 134418 (2012)] in this paper we provide an approach to systematically screen compounds of a given Heusler family to predict ones that can yield giant magnetocaloric effect driven by a first-order magnetostructural transition. We apply this approach to two Heusler series $Ni_{2-x}Fe_xMn_{1+z-y}Cu_ySb_{1-z}$ and $Ni_{2-x}Co_xMn_{1+z-y}Cu_ySb_{1-z}$ obtained by cosubstitution at Ni and Mn sites. We predict four new compounds with potentials to achieve the target properties. Our computations of the thermodynamic parameters relevant for magnetocaloric applications show that the improvement in the parameters in the predicted cosubstituted compounds can be as large as four times in comparison to the off-stoichiometric Ni-Mn-Sb and a compound derived by single substitution at the Ni site where magnetocaloric effects have been observed experimentally. This work establishes a protocol to select new compounds that can exhibit large magnetocaloric effects and demonstrate cosubstitution as a route for more flexible tunability to achieve outcomes better than the existing ones.

I. INTRODUCTION

The development of magnetic refrigeration, a new solid-state refrigeration technology, based on the magnetocaloric effect (MCE), continues to attract considerable attention worldwide due to its environmentally friendly nature, higher energy efficiency, lower mechanical noise, and simple mechanical construction, in comparison with conventional technology based on gas compression/expansion [1–3]. The underlying magnetocaloric effect (MCE) is measured in terms of isothermal magnetic entropy change (ΔS_{mag}) and/or adiabatic temperature change (ΔT_{ad}) that require large variations in the material's magnetization with temperatures. In the magnetic refrigerators, Gd has been considered as a benchmark material due to the discovery of significant magnetocaloric effect in it, an outcome of a second-order ferromagnetic to paramagnetic transition close to room temperature [4]. However, giant effect is generally observed in materials which undergo a first-order magnetostructural transition, i.e., a structural phase transition, coupled with a magnetic one [5–20]. Magnetic refrigeration near room temperature is of special interest because of its social and economic benefits. From this point of view, the continuous search of new solid-state magnetic refrigerants that could exhibit a giant MCE, in an appropriate temperature range, as well as the improvement of the existing ones, have been the focus of research in this area.

Among MCE materials, shape memory Heusler compounds are of great interest as they exhibit large MCE, and their transition temperatures can be easily tuned. The origin of their large MCE is the first-order martensitic phase transition (MPT) from a high temperature cubic austenite phase to a low temperature low symmetry phase, a large magnetization change occurring simultaneously. One of the compounds in the Heusler family which recently showed promising MCE is the off-stoichiometric Mn-excess Sb-deficient Ni-Mn-Sb where magnetostructural transition and significant magnetocaloric effect were observed near room temperature [21–23].

With an aim to improve the MCE in this family of compounds, some recent investigations have also been carried out, by substituting the Fe and Co atoms at Mn and Ni sites, respectively, resulting in large positive values of ΔS_{mag} [23–26]. Though the transition metal substituted Ni-Mn-Sb Heusler compounds turn out to be useful materials exhibiting giant MCE, one major disadvantage is that upon substitution, the working temperature, i.e., the martensitic transformation temperature (T_M), falls below room temperature. This is not desirable for operational purposes. In some recent studies, the strategy of substitution of at least two 3d elements simultaneously (cosubstitution) has been found to be useful in achieving the important magnetic and structural properties with better tuning and adaptability [27–29]. In a recent work [30] we explored potential room-temperature magnetocaloric materials in two cosubstituted families $Ni_{2-x}Fe_xMn_{1+z-y}Cu_ySb_{1-z}$ (Fe@Ni-Cu@Mn) and $Ni_{2-x}Co_xMn_{1+z-y}Cu_ySb_{1-z}$ (Co@Ni-Cu@Mn). We found that for a certain range of compositions, there is no structural transformation down to the low temperature indicating that the MCE is purely due to second-order magnetic phase transition. We also found that large magnetic moments and T_c, the Curie temperature, close to room temperatures can be easily achieved by tuning the compositions, along with a significant MCE. These indicated a delicate balance of the concentrations of different constituents and easy tunability of properties in this family. Armed with this

[*]sheuly.ghosh@iitg.ac.in
[†]subhra@iitg.ac.in

information, in the present work, we focused on the composition ranges that were not covered in Ref. [30]. A martensitic phase transformation (MPT) occurs in cosubstituted Ni-Mn-Sb compounds with those compositions. We aimed to explore whether a giant MCE due to magnetostructural coupling can be predicted in these compositions along with near room temperature T_M. Using a thermodynamic model in conjunction with first-principles electronic structure calculations, we made comparisons with the systems already explored experimentally and provided predictions of new compounds, yet to be realized experimentally, that can exhibit significantly large MCE. This study established a systematic way to use the information on structural and magnetic properties obtained from first-principles calculations to screen the materials that are potential ones with target properties and the robustness of the formalism to accurate predictions of new compounds.

II. METHOD OF CALCULATION AND COMPUTATIONAL DETAILS

Most of the literature on MCE, particularly for Heusler compounds, is experimental in nature. Very few theoretical studies of MCE in the framework of molecular-field approximation [31–33], bond proportion model [34], and Monte Carlo simulations [35–39] have been reported. Tackling the problem using theoretical tools is a difficult one as the task to obtain all phases in a self-consistent way is quite demanding. This requires the equilibrium, *ab initio* evaluation of all magnetic exchange parameters and comparison of free energies, for each structure (austenite and martensite) at different temperatures. Avoiding all the above mentioned complex and time-consuming calculations, a unified description of structural and associated first-order magnetic phase transition has been presented in literature, successfully for Ni-Mn based Heusler compounds, by using a simple model Hamiltonian consisting of tunable parameters [36–38,40–44]. The Hamiltonian allowed one to explore the richness of the phase diagram. The observed qualitative and quantitative behavior of MCE quantities turned out to be in very good agreement with experiments. Therefore, we have adopted the same method in this work.

A. First-principles methods and computational details

We have used the first-principles electronic structure calculations to gain information on the phase stability of the compounds explored and their magnetic properties. The electronic structure calculations were done with a spin-polarized density functional theory (DFT) based projector augmented wave (PAW) method as implemented in the Vienna *ab initio* simulation package (VASP) [45–47]. The valence electronic configurations used for the Mn, Fe, Co, Ni, Cu, and Sb PAW pseudopotentials are $3d^6 4s$, $3d^7 4s$, $3d^8 4s$, $3d^8 4s^2$, $3d^{10} 4s$, and $5s^2 5p^3$, respectively. For all calculations we used the Perdew-Burke-Ernzerhof implementation of a generalized gradient approximation for the exchange-correlation functional [48]. An energy cutoff of 550 eV, and a Monkhorst-Pack $11 \times 11 \times 11$ k mesh, were used for self-consistent calculations. The convergence criteria for the total energies and

the forces on individual atoms were set to 10^{-6} eV and 10^{-2} eV/Å, respectively.

The stabilities of the compounds against decomposition into its components were checked by computing the formation energies:

$$E_f = E_{\text{tot}} - \sum_i n_i E_i. \quad (1)$$

E_{tot} is the total electronic energy of the systems, i represents the atoms in the unit cell, and n_i is the concentration of the ith atom. E_i is the total energy of the element i in its bulk ground state.

To compute the Curie temperature T_c of a compound, we first calculated the magnetic pair exchange parameters using multiple scattering Green function formalism (KKR) as implemented in SPRKKR code [49]. In here the spin part of the Hamiltonian was mapped to a Heisenberg model,

$$H = -\sum_{\mu,\nu} \sum_{i,j} J_{ij}^{\mu\nu} \mathbf{e}_i^\mu . \mathbf{e}_j^\nu. \quad (2)$$

μ, ν represent different sublattices, i, j represent atomic positions, and $\mathbf{e}_i^\mu$ denotes the unit vector along the direction of magnetic moments at site i belonging to sublattice μ. The $J_{ij}^{\mu\nu}$'s were calculated from the energy differences due to infinitesimally small orientations of a pair of spins within the formulation of Liechtenstein *et al.* [50]. In order to calculate the energy differences by the SPRKKR code, a full potential spin-polarized scalar relativistic Hamiltonian with angular momentum cutoff $l_{\max} = 3$ was used along with a converged k mesh for Brillouin zone integrations. The Green's functions were calculated for 32 complex energy points distributed on a semicircular contour. The energy convergence criterion was set to 10^{-5} eV for the self-consistent cycles. These exchange parameters were then used for the calculation of T_c. The Curie temperatures were estimated with two different approaches: the mean-field approximation (MFA) [51,52] and the Monte Carlo simulation (MCS) method [53–55]. Details of the calculations using these methods are given in Ref. [56].

B. Calculation of MCE parameters using thermodynamic model

The Monte Carlo simulation is an appropriate tool to use the zero-temperature *ab initio* calculations for computing properties at finite temperatures. Here we have used Monte Carlo simulation on a model Hamiltonian to estimate the MCE parameters, i.e., isothermal change in magnetic entropy (ΔS_{mag}) or adiabatic temperature change (ΔT_{ad}) due to the application of a magnetic field. The model Hamiltonian was chosen such that it accommodates, along with magnetic and structural degrees of freedom, the coupling between the two [37,38,41,42].

The model Hamiltonian (H) consists of three parts: (a) the magnetic contribution due to the magnetic degrees of freedom of the system H_m; (b) the elastic contribution due to the structural transformation from cubic to tetragonal phases H_{els}; and (c) the contribution arising from the coupling of magnetic and structural interactions H_{int}:

$$H = H_m + H_{\text{els}} + H_{\text{int}}. \quad (3)$$

The magnetic subsystem is described by a mixed q-states Potts model [38,40,42,57], which allows for both first- and second-order phase transitions, where q is the number of spin states for magnetic atoms:

$$H_m = -\sum_{\langle i,j \rangle}^{NN} J_{ij}\delta_{S_i, S_j} - g\mu_B\mu_0 H_{\text{ext}} \sum_i^N \delta_{S_i, S_g}. \tag{4}$$

Here the first term represents the magnetic interactions at different lattice sites; $J_{i,j}$ being the exchange parameters involving sites i and j, S_i the spin defined on the lattice site $i = 1, 2, \ldots, N$, and N the total number of atoms considered in the simulation cell. The second term represents the coupling of the spin system to the external magnetic field H_{ext} along the direction of ghost spin variable S_g. μ_B is the Bohr magneton, and g is the Lande factor (here $g = 2$).

The degenerate Blume-Emery-Griffiths (BEG) model [58,59], which allows one to describe the interaction between the elastic variables, was used to address the mutual influence of magnetic ordering and structural transitions. The energy of the system undergoing structural transformation can be represented by

$$\begin{aligned} H_{\text{els}} = &-J \sum_{\langle i,j \rangle}^{NN} \sigma_i\sigma_j - K \sum_{\langle i,j \rangle}^{NN} \left(1 - \sigma_i^2\right)\left(1 - \sigma_j^2\right) \\ &- k_B T \ln(p) \sum_i \left(1 - \sigma_i^2\right) \\ &- K1 g\mu_B\mu_0 H_{\text{ext}} \sum_i^{NN} \delta_{\sigma_g \sigma_i} \sum_{\langle i,j \rangle}^{NN} \sigma_i\sigma_j, \end{aligned} \tag{5}$$

where σ is the strain parameter and denotes the structural state of the lattice site which takes the value 0 for cubic or undistorted state, and $+1$ or -1 for the tetragonal or distorted state. J and K are structural exchange constants for tetragonal and cubic states, respectively, p is the degeneracy factor characterizing the number of tetragonal states, $K1$ is the dimensionless magnetoelastic interaction, and T is the temperature of the system. The third term accounts for the higher configurational entropy in the cubic phase. The last term accounts for the energy contribution due to the changes in the structural states under the influence of the external magnetic field. The structural states are coupled to the external magnetic field through the ghost spin state σ_g. The sign of the magnetoelastic parameter $K1$ indicates the favored structural state (cubic or tetragonal), in the presence of an external magnetic field. For $K1 > 0$, energy is removed from the system in a tetragonal state, so that the tetragonal (distorted) state is favored over cubic state by the external magnetic field, while for $K1 < 0$, energy is added to the system in a tetragonal state so that the cubic state is favored. In essence, $K1 > (<)0$ if T_M increases (decreases) in the presence of external magnetic field:

$$H_{\text{int}} = 2\sum_{\langle i,j \rangle}^{NN} U_{ij}\delta_{S_i, S_j} \left(\frac{1}{2} - \sigma_i^2\right)\left(\frac{1}{2} - \sigma_j^2\right) - \frac{1}{2}\sum_{\langle i,j \rangle}^{NN} U_{ij}\delta_{S_i, S_j}. \tag{6}$$

In the magnetoelastic part [Eq. (6)] of the Hamiltonian, the first term describes the effective coupling of magnetic sublattice to the modulation of the lattice, while the last term renormalizes the spin-spin interaction. U_{ij} is the magnetoelastic interaction parameter.

This Hamiltonian [Eq. (3)] was used for Monte Carlo calculations using the following procedure:

1. For all the magnetic and lattice sites in the supercell, values of initial spin (S_i) and strain (σ_i) were chosen as 1.

2. First, one arbitrary lattice site was chosen, and the initial elastic energy contribution ($H_{\text{els}}^{\text{initial}}$) from that site was calculated using Eq. (5). For $\sigma_i = 0$, the site's energy contribution was calculated on a cubic lattice, while for $\sigma_i = +1$ or $\sigma_i = -1$, the energy was calculated on a tetragonal lattice. This was also done while calculating the magnetic and coupled contributions of the Hamiltonian.

3. For the same site i, the strain parameter σ_i was changed randomly. The elastic energy of the new configuration $H_{\text{els}}^{\text{final}}$ was calculated. The change in the elastic energy of the system ($H_{\text{els}}^{\text{final}} - H_{\text{els}}^{\text{initial}}$) was then computed.

4. The new system configuration, i.e., the lattice with a new strain parameter on that particular site, was accepted or rejected based on the Metropolis algorithm [53,54,60]. If $H_{\text{els}}^{\text{final}} \leqslant H_{\text{els}}^{\text{initial}}$, the new system configuration was accepted; else a ratio R is calculated:

$$R = \exp\left[-\left(H_{\text{els}}^{\text{final}} - H_{\text{els}}^{\text{initial}}\right)/k_B T\right]. \tag{7}$$

A random number ($r; 0 < r < 1$) is generated, and if $R > r$, the new configuration was accepted.

5. The next step was to find the new spin state for site i. The total energy of the system H^{initial} was calculated using Eq. (3). The spin state of site i was then changed randomly, and the energy of the new configuration H^{final} was calculated. The new system configuration (site i with new spin parameter) was then accepted or rejected based on the Metropolis algorithm, as described in the previous step.

6. Steps 2–5 were then repeated by moving through the lattice sites. Once all the lattice sites were swept, one Monte Carlo step (MCS) was completed.

At a given temperature, the system was first equilibrated by repeating the above Monte Carlo steps. Then the average magnetization (m) and strain order parameter (ε) of the equilibrated system for a given temperature were calculated as

$$m = \frac{1}{N}\sum_i^n \frac{\left(q_i N_i^{\text{max}} - N_i\right)}{q_i - 1}, \tag{8}$$

$$\varepsilon = \frac{1}{N}\sum_i \sigma_i, \tag{9}$$

where i in Eq. (8) denotes a magnetic atom type, n is the total number of magnetic atom types, q_i is the total number of spin states of the atom of type i, N_i^{max} is the maximum number of atoms of type i with the same spin state, N_i is the total number of atoms of type i, and N is the total number of atoms in the system. The magnetic specific heat (C_{mag}), the magnetic entropy (S_{mag}), and total specific heat $C = C_{\text{lat}} + C_{\text{mag}}$ with lattice and magnetic contributions were then calculated. We have neglected the electronic part of the specific heat. For the lattice heat, we have used the standard Debye approximation. Finally, the magnetocaloric parameters, i.e., the isothermal

changes in magnetic entropy (ΔS_{mag}) and the adiabatic temperature change (ΔT_{ad}) due to the application of an external field, were calculated by Eqs. (13) and (14), respectively:

$$C_{mag}(T, H_{ext}) = \frac{1}{N} \sum_{i}^{N} \frac{\langle H^2 \rangle - \langle H \rangle^2}{k_B T^2}, \quad (10)$$

$$S_{mag}(T, H_{ext}) = \frac{1}{N} \int_0^T dT \frac{C_{mag}(T, H_{ext})}{T}, \quad (11)$$

$$C_{lat}(T, \Theta_D) = 9RN_i \left\{ 4\left(\frac{T}{\Theta_D}\right)^3 \int_0^{\Theta_D/T} dx \frac{x^3}{e^x - 1} \right.$$
$$\left. - \left(\frac{\Theta_D}{T}\right) \frac{1}{e^{(\Theta_D/T)} - 1} \right\}, \quad (12)$$

$$\Delta S_{mag}(T, H_{ext}) = S_{mag}(T, H_{ext}) - S_{mag}(T, 0), \quad (13)$$

$$\Delta T_{ad}(T, H_{ext}) = -T \frac{\Delta S_{mag}(T, H_{ext})}{C(T, H_{ext})}. \quad (14)$$

An important approximation has been made in this approach of computing the ΔS: the contributions from the lattice vibrations is neglected altogether. However, this is justified due to following: the isothermal entropy change because of lattice vibration (ΔS_{vib}) due to a change in the magnetic field, across the magnetostructural transitions, is not significant as long as the Debye temperature does not depend strongly on the magnetization and magnetic field, i.e., $S_{vib}(T, H_{ext}) \sim S_{vib}(T, 0)$. Experiments on Ni-Mn Heusler compounds have shown negligible contribution of the external magnetic field on the phonon dispersion [61]. Hence, as was done in existing literature [38,40], neglect of the contributions of lattice vibrations to entropy change is a valid approximation for the systems considered.

III. RESULTS AND DISCUSSIONS

In this work we investigated the two cosubstituted Mn-excess, Sb-deficient Ni-Mn-Sb families: (i) $Ni_{2-x}Fe_x Mn_{1+z-y}Cu_y Sb_{1-z}$ (denoted as Fe@Ni-Cu@Mn) and (ii) $Ni_{2-x}Co_x Mn_{1+z-y}Cu_y Sb_{1-z}$ (denoted as Co@Ni-Cu@Mn). As mentioned in Sec. I, our motivation was to find compounds that give rise to large MCE driven by first-order magnetostructural transition. In order to model the compounds that have multisublattice chemical disorder, we have considered a 16 atom conventional cubic unit cell. This unit cell mimics the high temperature austenite ($L2_1$ Heusler) phase of the systems (space group 225). The consequence of the cell size is the inability to model compositions with arbitrary x, y, or z. Each one of the three variables can be changed by an amount of 0.25 only. The choice of the composition range to achieve ones with the target properties is crucial. For this we took recourse to our previous works on the same system [30,62]. Based upon the findings there, we restricted the value of x to 0.25, and the range of z between 0.50 and 0.75. The variable y is constrained to be less than or equal to the value of z. The compounds with these compositions are expected to exhibit a martensitic phase transformation.

Since site occupancies in the compounds do not always follow a regular pattern (the excess atoms occupying the sites of deficient atoms in the reference system) [55,63–67] affecting the MCE properties as a consequence, we first found out the

minimum energy configuration for each composition by comparing the total energies of configurations with different site occupancy patterns and magnetic configurations. We found that the substituting Fe/Co atoms prefer to occupy the Ni sites, whereas the Cu atoms prefer to occupy the Sb sites, the same as found out in Ref. [30]. We also found that depending upon the composition, two types of magnetic configurations are found leading to minimum total energy; FM, where the two types of Mn can align parallel, and FIM, where the two types of Mn can align antiparallel.

After fixing the lowest energy configurations, we first calculated the formation energies for all the compounds. Negative values of the formation energy for each of the composition (Table I) indicated their stability against decomposition into its constituent elements. Subsequently, the following criteria were used to screen materials further to narrow down the ones which are potential large MCE materials:

(i) The materials should possess a high magnetic moment in their austenite phases.

(ii) The martensitic transformation temperature (T_M) should be near room temperature or higher than that.

(iii) The MPT should be associated with a substantial change in magnetization. In other words, a magnetic structure in the martensite phase different than that in the austenite phase would be advantageous.

(iv) The second-order magnetic transition temperature, i.e., the Curie temperature (T_c^A) in the austenite phase, should be close to the martensitic transformation temperature (T_M). This would lead to a large change in entropy due to near simultaneous magnetic and structural transition. Otherwise, T_c^A should be higher than T_M so that the MPT can occur in a magnetically ordered phase.

In what follows, we present and analyze the results on the variations in the magnetic moments in the austenite phases, the relative stabilities of the structural phases, and variations in the T_M and the variations in T_c^A with changes in the compositions by systematic variations in x, y, and z. The analysis helps us in the prediction of new compounds that have potentials to exhibit large MCE. In here we first understand the trends in the physical quantities due to cases with single substitution. For that, we extended the range of x up to 0.75 in all substituted compounds. The outcome of the cosubstituted cases can be understood in the light of the results for single substituted compounds.

A. Magnetic moment in austenite phase

A correlation between enhancement of magnetization in the austenite phase and a large MCE for Ni-Mn-Sb system could be observed in the experiments [23,24]. For $Ni_{1.8}Co_{0.2}Mn_{1.52}Sb_{0.48}$ [23], an enhanced magnetic moment in the austenite phase has been observed due to the Co substitution at Ni site. Subsequently, a large positive MCE was observed in the system, presumably an artifact of magnetoelastic coupling. In general, a significant enhancement of magnetic moment in the austenite phase leads to a possibility of large ΔM, the difference in magnetization between austenite and martensitic phases, the key to a first-order magnetostructural transition. We therefore focus on finding the possibility of enhancement of magnetic moment in austenite

TABLE I. Calculated values of equilibrium lattice constant (a_0), formation energies (E_f), and total magnetic moment (M_A) of the systems under considerations in their austenite phases. The corresponding ground state magnetic configurations are shown. The total energy difference (ΔE) between the austenite($L2_1$) and the martensite(tetragonal) phases, the equilibrium value of tetragonal distortion (c/a), the differences in magnetic moments between the austenite and martensite phases (ΔM), the mean-field approximated ($T_c^{A(\mathrm{MFA})}$), and Monte Carlo simulated ($T_c^{A(\mathrm{MCS})}$) Curie temperatures in the austenite phases are also shown. Boldface indicates the reference compositions around which experimental studies [22,23,69] are available. The compositions shown within the borders are found to satisfy the criteria for considering them as efficient giant magnetocaloric materials with improved MCE properties than the reference ones.

Ni$_{2-x}$A$_x$Mn$_{1.50-y}$Cu$_y$Sb$_{0.50}$ ($z = 0.50$)

Composition		Mag.	a_0	E_f	M_A	ΔE	c/a	$\lvert \Delta M \rvert$	$T_c^{A(\mathrm{MFA})}$	$T_c^{A(\mathrm{MCS})}$
x	y	Config.	(Å)	(eV/f.u.)	(μ_B/f.u.)	(meV/atom)		(μ_B/f.u.)	(K)	(K)
0.00	**0.00**	**FIM**	5.94	−0.552	1.71	27.64	1.34	0.16	397	422
A = Fe										
0.25	0.00	FIM	5.92	−0.450	2.09	10.68	1.29	0.18	351	370
0.25	0.25	FIM	5.91	−0.386	3.29	4.45	1.24	0.08	297	340
0.25	0.50	FM	5.90	−0.317	4.44	No MPT	–	–	327	300
A = Co										
0.25	**0.00**	**FIM**	5.93	−0.670	1.99	20.97	1.30	0.04	392	410
0.25	0.25	FIM	5.91	−0.620	3.22	16.91	1.28	0.23	333	401
0.25	0.50	FM	5.90	−0.567	4.42	10.93	1.25	0.19	355	399

Ni$_{2-x}$A$_x$Mn$_{1.75-y}$Cu$_y$Sb$_{0.25}$ ($z = 0.75$)

Composition		Mag.	a_0	E_f	M_A	ΔE	c/a	$\lvert \Delta M \rvert$	$T_c^{A(\mathrm{MFA})}$	$T_c^{A(\mathrm{MCS})}$
x	y	Config.	(Å)	(eV/f.u.)	(μ_B/f.u.)	(meV/atom)		(μ_B/f.u.)	(K)	(K)
0.00	0.00	FIM	5.86	-0.470	0.69	55.32	1.36	0.15	348	290
A = Fe										
0.25	0.00	FM	5.89	−0.352	7.71	41.22	1.38	6.27	498	406
0.25	0.25	FIM	5.84	−0.312	2.17	35.30	1.35	0.19	241	120
0.25	**0.50**	**FM**	5.83	−0.240	5.54	23.58	1.33	3.33	448	362
0.25	**0.75**	**FM**	5.81	−0.167	4.43	24.22	1.32	1.22	408	320
A = Co										
0.25	**0.00**	**FM**	5.90	−0.615	7.75	37.25	1.34	6.78	519	450
0.25	**0.25**	**FM**	5.87	−0.576	6.66	31.87	1.32	4.66	489	460
0.25	0.50	FM	5.84	−0.525	5.62	12.20	1.28	2.53	464	450
0.25	0.75	FM	5.81	−0.468	4.53	4.40	1.24	0.27	431	425

phases of Ni-Mn-Sb compounds upon substitution by $3d$ elements at different sites. We present the results on total and atomic magnetic moments in Figs. 1 and 2. The panels (a)–(c) in each of the two figures show results for single substitution while (d) and (e) show results for cosubstitution. All results in Fig. 1 are for compounds with $z = 0.5$ that is with 50% excess Mn (with respect to stoichiometric Ni$_2$MnSb) while those in Fig. 2 are with $z = 0.75$. If we first look at the compounds with single substitution (Table 1, Ref. [56]), we find that irrespective of z, Cu substitution at the Mn site allows the total moment to increase linearly with the Cu content y. This is due to the fact that the atomic moments of both Mn atoms stay nearly the same and that the gradual replacement of Mn2 atoms by Cu reinforces the moment since Mn2, being aligned antiparallel to Mn1, was reducing the total moment. When Fe or Co substitutes Ni, irrespective of the value of z, the behavior of magnetic moment with the concentration of Fe or Co, x, is qualitatively identical in the sense that a monotonic variation with x is either preceded or followed by a discontinuous jump at a critical value of x; the difference being in the critical value. Such a discontinuous jump with at least twofold increase in

the total moment occurs due to the change in the magnetic structure from FIM to FM, driven by the orientations of the Mn atoms. The variations in the moments for cosubstitution with x fixed at 0.25, turn out to be the combined behavior of the two single-substituted cases, Fe or Co substituting Ni and Cu substituting Mn. Due to the presence of higher concentration of Mn2 atoms in compounds with $z = 0.75$, in comparison to those with $z = 0.5$, the overall moments in the former cosubstituted compounds are higher than that in the later (Table I). The inference from these results is that the compositions with $z = 0.75$ may provide higher values of ΔM and thus better MCE than compounds with composition having $z = 0.5$, closest to the one on which experiments have been performed.

B. Martensitic transformation and magnetic structures across structural phases

Next, we investigate whether MPT occurs in our systems of investigation. To this end, we distort the austenite $L2_1$ structure along the z axis by keeping the volume at the equilibrium
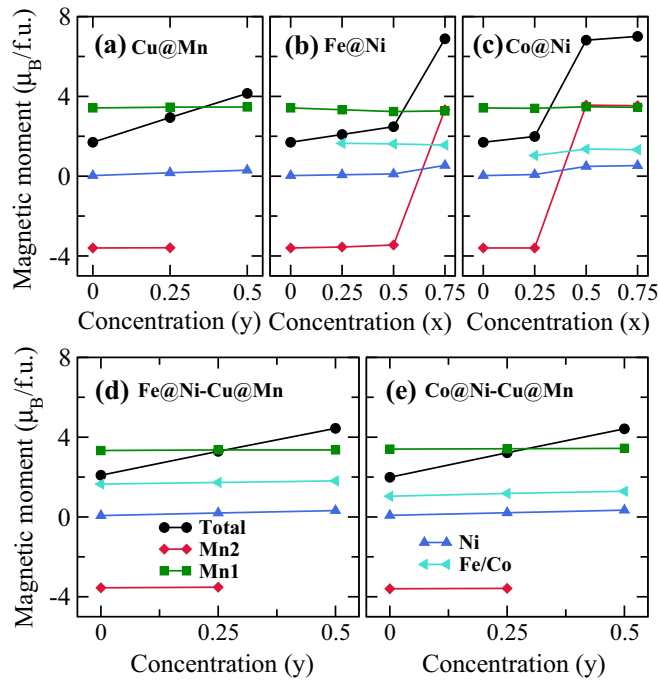
FIG. 1. Variations in the calculated total and atomic magnetic moments (in μ_B/f.u.) with (a) y ($x = 0$), (b) and (c) x ($y = 0$), and (d) and (e) y ($x = 0.25$) for $\mathrm{Ni_{2-x}Fe_xMn_{1+z-y}Cu_ySb_{1-z}}$ (Fe@Ni-Cu@Mn) and $\mathrm{Ni_{2-x}Co_xMn_{1+z-y}Cu_ySb_{1-z}}$ (Co@Ni-Cu@Mn) systems in their austenite phases. z value is kept at 0.5 throughout. Mn1 and Mn2 denote Mn atoms at its own site and at other sites in $L2_1$ structure, respectively.

FIG. 2. Variations in the calculated total and atomic magnetic moments (in μ_B/f.u.) with (a) y ($x = 0$), (b) and (c) x ($y = 0$), and (d) and (e) y ($x = 0.25$) for $\mathrm{Ni_{2-x}Fe_xMn_{1+z-y}Cu_ySb_{1-z}}$ (Fe@Ni-Cu@Mn) and $\mathrm{Ni_{2-x}Co_xMn_{1+z-y}Cu_ySb_{1-z}}$ (Co@Ni-Cu@Mn) systems in their austenite phases. z is kept at 0.75 throughout. Mn1 and Mn2 denote Mn atoms at its own site and at other sites in $L2_1$ structure, respectively.

value of the austenite phase and compute the total energy of the system as a function of the tetragonal distortion given by (c/a). Typical profiles of compounds undergoing MPT will have their minima at $(c/a) \neq 1$. For all compositions we calculated the energy profiles as a function of tetragonal distortion. The results are shown in Fig. 3. The results suggest that all the considered compounds undergo MPT, a requirement for further consideration. However, for compounds with higher Mn content ($z = 0.75$), the magnetic ground states of the austenite phases are different than those in the martensitic phases except at the compound where $y = 0.75$. In all such cases, the austenite phase has FM magnetic structure (Table I), while the martensitic phase has FIM magnetic structure. The results in Figs. 3(c) and 3(d) corroborate this. A consequence of this is a large value of ΔM (Table I) for the compounds with $z = 0.75$ as compared to those with $z = 0.5$. This makes the compounds with $z = 0.75$ potentially better to realize large MCE.

In order to make sure that this is indeed so, we looked at the variations in ΔE, the energy difference between the austenite and martensite phases in their respective ground states. The results for single-substituted compounds are shown in Figs. 4(a)–4(c) while those for cosubstituted ones are shown in Figs. 4(d) and 4(e). The ΔE values are also listed in Table I. In literature, ΔE is routinely used to predict the martensitic transformation temperature (T_M) [55,62,65,67,68]. Here we have used it first to understand the trends in the T_M so that compositions with higher T_M can be screened. From Fig. 4 we
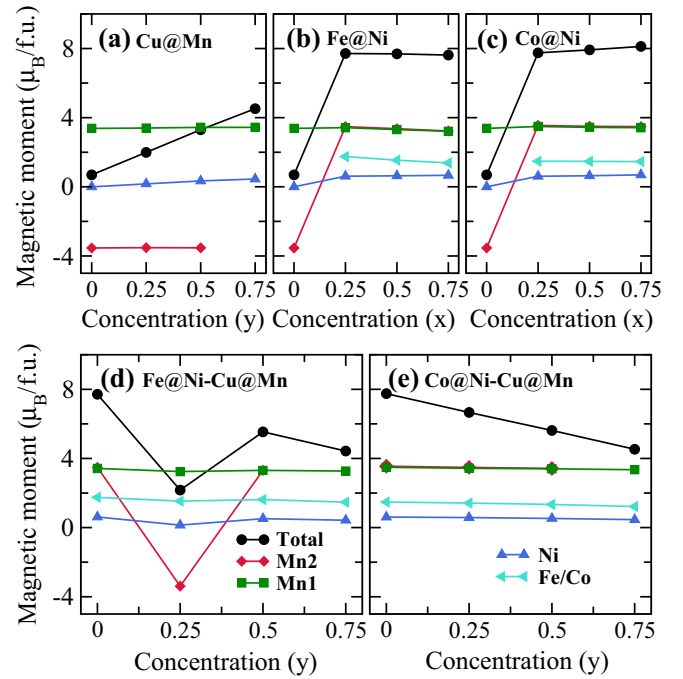
find that the trends in variations of ΔE with compositions in cases of the cosubstituted compounds can be correlated with the trends in case of single-substituted ones. A general trend of $z = 0.75$ compounds having higher ΔE and thus higher T_M can be immediately inferred. Therefore, in both the counts of larger ΔM and higher T_M, the compounds with Mn content as high as 1.75 can be considered promising to obtain large MCE.

C. Curie temperature in austenite phase

In Fig. 5 we present the calculated Curie temperature (T_c^A) in the austenite phase for all the compositions, using both the mean-field approximation and the more accurate Monte Carlo simulation method. The results for single-substituted compounds are presented in Figs. 5(a)–5(c), and those for the cosubstituted compounds are presented in Fig. 5(d) and 5(e). The T_c^A values for all the cosubstituted compositions are listed in Table I. Here, too, the trends of variations in T_c^A for cosubstituted compounds can be correlated to the trends in cases of single substitutions. Overall it can be concluded that for cosubstituted systems, the T_c^A values are higher for compounds with $z = 0.75$. This is more prominent for Co and Cu cosubstituted systems (Co@Ni-Cu@Mn). Thus cosubstituted Co@Ni-Cu@Mn family with $z = 0.75$ have more possibility of fulfilling the target properties of a giant magnetocaloric material.
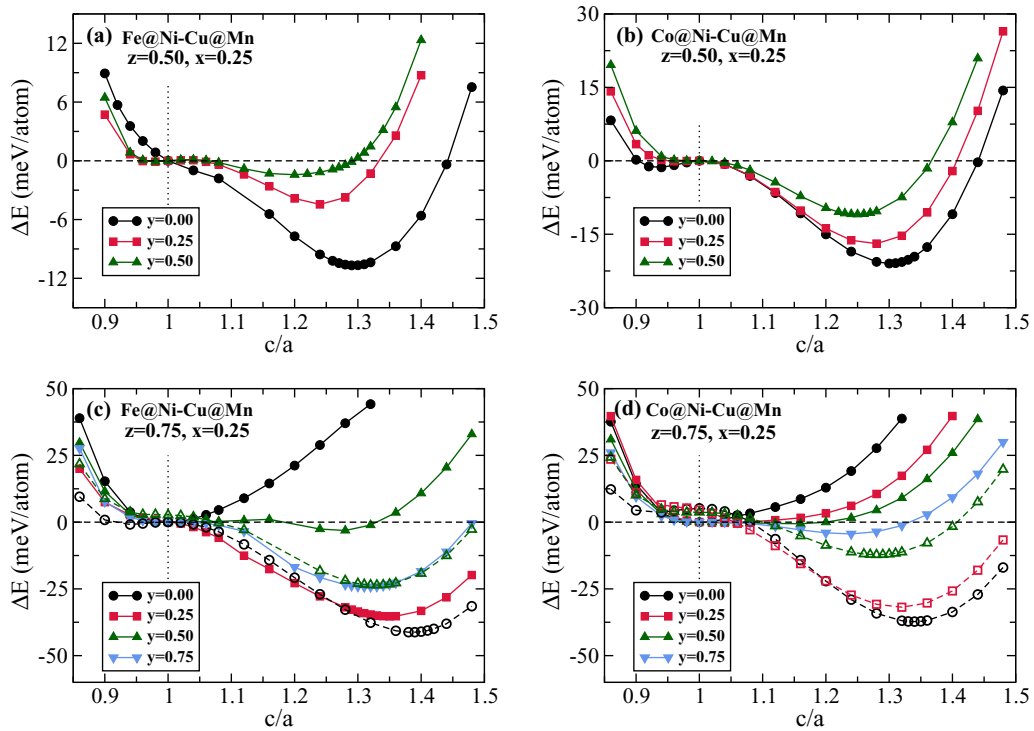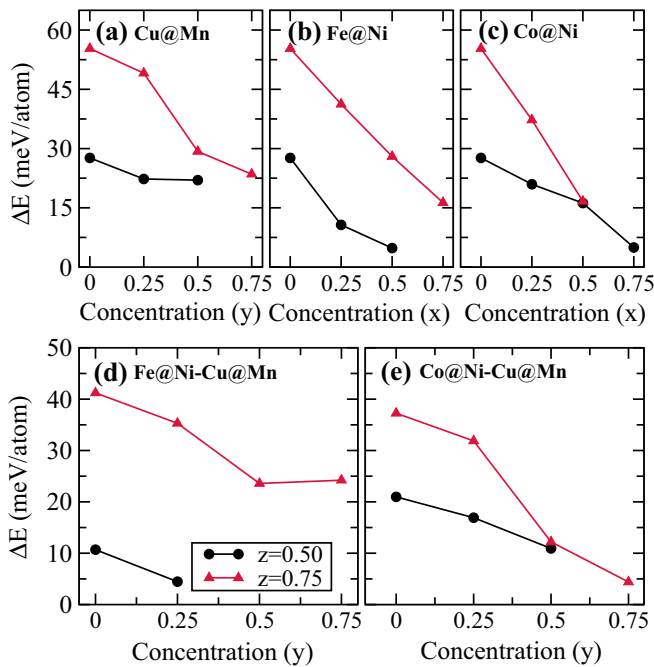
FIG. 3. The variations of total energy difference (ΔE) between the austenite($L2_1$) and the martensite(tetragonal) phases as a function of tetragonal distortion, i.e., c/a ratio in $Ni_{2-x}(Fe/Co)_x Mn_{1+z-y}Cu_y Sb_{1-z}$ [(Fe/Co)@Ni-Cu@Mn] compounds for different y with (a) and (b) $z = 0.50$ and (c) and (d) $z = 0.75$. x is fixed at the value 0.25 for all calculations. The magnetic configurations considered in each case is given in Table I. The solid curves are for cases where magnetic configurations considered are the same in both structural phases. The dotted curves in (c) and (d) are for cases where the magnetic configurations in the tetragonal phases are different from those in the Heusler phases and provide minimum total energies.

FIG. 4. Variations in total energy difference ΔE between the austenite($L2_1$) and the martensite(tetragonal) phases with (a) y ($x = 0$), (b) and (c) x ($y = 0$), and (d) and (e) y ($x = 0.25$) for $Ni_{2-x}(Fe/Co)_x Mn_{1+z-y}Cu_y Sb_{1-z}$ compounds with different values of z.
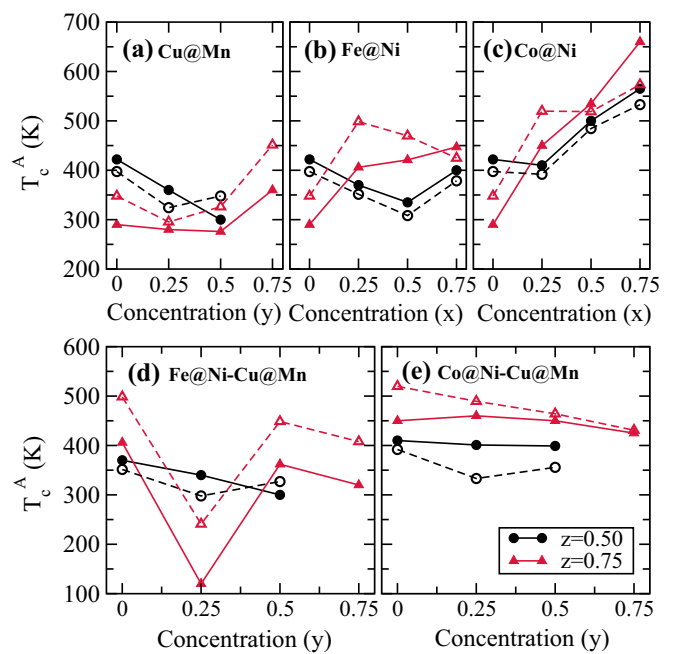

FIG. 5. Variations in calculated Curie temperatures (T_c^A) in austenite phases with concentration (a) y ($x = 0$), (b) and (c) x ($y = 0$), and (d) and (e) y ($x = 0.25$) for $Ni_{2-x}(Fe/Co)_x Mn_{1+z-y}Cu_y Sb_{1-z}$ systems with different z. Closed symbols and open symbols represent results calculated by Monte Carlo simulation (MCS) and mean-field approximation (MFA) methods, respectively.

D. Prediction of new compounds

Based upon the results presented in the previous three subsections, we are now in a position to predict new compounds which can exhibit better MCE properties than that observed in the experimentally synthesized compounds. To this end we first consider the compounds $Ni_2Mn_{1.5}Sb_{0.5}$ (i.e., $x = 0.00$, $y = 0.00$, $z = 0.50$) and $Ni_{1.75}Co_{0.25}Mn_{1.5}Sb_{0.5}$ (i.e., $x = 0.25$, $y = 0.00$, $z = 0.50$) (boldfaced in Table I) as the reference ones with respect to which we assess the improvement in properties. These compounds are chosen as the compositions in these compounds are very close to the experimentally investigated ones [22–25,69–71]. Comparing all the quantities, we predict four compositions (bold bordered in Table I), two in the Fe@Ni-Cu@Mn family, and the other two in the Co@Ni-Cu@Mn family. In all the cases, $z = 0.75$ that is the Mn atom is in excess by 75% in comparison to perfectly ordered Ni_2MnSb, the parent compound. For all the predicted compositions, the ground state magnetic configuration in the austenite phase is the FM one, where the two types of Mn atoms are aligned parallel, leading to larger magnetic moments compared to the reference systems. For these compounds, large values of change in magnetization (ΔM), compared to the reference compounds, are observed during the martensitic phase transformation. Finally, the conditions that the martensitic transformation temperature (T_M) and Curie temperature (T_c^A) either should nearly coincide or T_c^A should be higher than T_M, are satisfied for the predicted compounds. In order to establish this, we have made an estimation of T_M the following way: the value of ΔE corresponding to $Ni_{1.75}Co_{0.25}Mn_{1.50}Sb_{0.50}$ composition is mapped to the experimental martensitic transformation temperature (T_M) value of 262 K, found for a compound with almost same composition $Ni_{1.8}Co_{0.2}Mn_{1.5}Sb_{0.5}$ [23]. Using this mapping we found that approximate values of T_M are 294, 302, 465, and 398 K for $Ni_{1.75}Fe_{0.25}Mn_{1.25}Cu_{0.5}Sb_{0.25}$, $Ni_{1.75}Fe_{0.25}MnCu_{0.75}Sb_{0.25}$, $Ni_{1.75}Co_{0.25}Mn_{1.75}Sb_{0.25}$, and $Ni_{1.75}Co_{0.25}Mn_{1.50}Cu_{0.25}Sb_{0.25}$, respectively. A look at Table I, along with these mapped values, shows that the above mentioned conditions are satisfied for all four.

E. Computation of the MCE parameters

After screening the compounds, most suitable to exhibit giant MCE, we aimed at the calculations of the MCE parameters ΔS_{mag} and ΔT_{ad} to establish our predictions. Since there is no experimental result to compare in cases of the new cosubstituted compounds, it is imperative that our approach of using the DFT, in conjunction with the proposed model Hamiltonian, is validated. To this end we used our approach to compute the MCE parameters for two compounds: $Ni_2Mn_{1.52}Sb_{0.48}$ and $Ni_{1.8}Co_{0.2}Mn_{1.52}Sb_{0.48}$ where experimental results are available [22,23]. After validation we computed the MCE parameters for $Ni_{1.75}Co_{0.25}Mn_{1.50}Cu_{0.25}Sb_{0.25}$, one of the compounds predicted. Due to the huge computational cost involved in cosubstituted compounds with multisublattice disorder, we restricted ourselves to only one out of the four new predicted compounds.

The compound $Ni_2Mn_{1.52}Sb_{0.48}$ was considered first. The Monte Carlo calculations were done using a simulation domain consisting of 8192 atoms obtained by replicating the unit cell, containing 16 atoms, eight times in each direction. The Mn2 atoms are randomly distributed on the Sb sublattices. The final simulation domain contains 983 Sb, 1065 Mn2, 2048 Mn1, and 4096 Ni atoms.

The magnetic exchange parameters J_{ij} in Eq. (4) were obtained from Figs. 1(a) and 1(b), Ref. [56]. The magnetic spin states (q) for Ni, Mn2, and Mn1 atoms were taken as 3, 6, and 6, respectively, in accordance with the studies on other Heusler systems [41,42]. The spin state of each magnetic atom site (S_i) were chosen randomly by generating a random number between 0 and 1 ($0 \leqslant r \leqslant 1$) and selecting the state as: if $0 \leqslant r \leqslant l/3$, then $q_{Ni} = l$, $l = 1, 2, 3$, and if $0 \leqslant r \leqslant k/6$, then $q_{Mn1(Mn2)} = k$, $k = 1, 2, 3,...,6$. We considered lattice sites up to the third coordination shells for Mn1-Mn1, Mn2-Mn2, and Mn1-Mn2 pairs, and up to the first-coordination shell for Mn1(Mn2)-Ni and Ni-Ni atom pairs in the summation. For elastic part of the Hamiltonian [Eq. (5)], the summation was taken over the pairs up to the second-coordination shell. A similar procedure, as for choosing S_i values, had been used to assign the σ_i values randomly. Values of structural constants J and K were chosen such that the martensitic transformation temperature (T_M) could be adjusted around the experimental T_M, which is around room temperature ($\approx$300 K) [22,70]. The constraint of $K/J \leqslant 0.5$ was imposed to get rid of any premartensitic phase. Although J and K could be obtained from *ab initio* calculations, we used a simple procedure of tuning to reduce the complexity as well as computational cost. This had been followed in other investigations [38,40] too. The degeneracy factor (p) for the cubic phase was taken as 2, since the cubic phase can distort along one of the three directions (here along the z direction). The $K1$ was chosen to be negative since it was experimentally observed that T_M decreased under application of external magnetic field. The negative $K1$ fixed the ghost deformation state σ_g to -1. The value of $K1$ was chosen such that the maximum magnetic entropy change is obtained around the experimental martensitic transformation temperature. In the magnetoelastic interaction part [Eq. (6)], the interaction parameters U_{ij} in cubic (U_c) and tetragonal (U_t) phases were tuned in such a way that the Curie temperature in the austenite phase is obtained around the experimental Curie temperature (350 K for the compound considered).

Thus, with an initial guess of J and K values, we adjusted the T_M to bring it closer to the experimental value. Once a reasonable T_M is obtained, we tuned the parameter U_{ij} in both structural phases to obtain the experimental Curie temperature. These are done by adjusting the coordination shells over which summations are done. These were done in the absence of an external magnetic field, i.e., $H_{ext} = 0$. Then we applied an external field of 5 T and tuned the $K1$ parameter so that T_M shifts in the direction observed in the experiment. This ensured a correct behavior of magnetic entropy change ΔS_{mag} as a function of temperature and ΔS_{mag}^{max} is achieved around the experimental T_M. Here, depending on the sign of $K1$, ghost deformation state σ_g was chosen. The simulation started with the initial values of σ_i as 1 for all the lattice sites and S_i, S_g as 1 for the magnetic atoms. The final values of all the parameters are presented in Table II. For each temperature step, 2×10^5 MC steps were performed. The system was

TABLE II. Values of structural, magnetoelastic, and coupling parameters that are used in the present study for $Ni_{2-x}Co_xMn_{1+z-y}Cu_ySb_{1-z}$ compounds.

Concentrations			Parameters				
			J	K	U_c	U_t	
x	y	z	(meV)	(meV)	(meV)	(meV)	$K1$
0.00	0.00	0.52	1.67	0.25	1.36	3.54	−0.25
0.20	0.00	0.52	1.67	0.42	7.56	14.24	−0.8
0.25	0.25	0.75	2.00	0.32	7.56	14.24	−0.4

equilibrated for 1×10^5 MC steps, and the data, then, were collected for 10^5 steps. For each temperature step, energy of the system (H), magnetization (m), and structural distortion (ε) were averaged over 1000 data points collected after every 100 MC steps. These averaged quantities were then used to calculate the various thermodynamic quantities using equations, given in Sec. II B.

Under zero field, the strain order parameter (ε) shows the structural transformation from austenite (undistorted phase with $\varepsilon = 0$) to martensite phases (distorted phase with $\varepsilon = 1$) with decreasing temperature [Fig. 6(a)]. The transformation occurs around 300 K, which is in good agreement with the experimental T_M. The magnetic order parameter (m) is almost zero at high temperatures indicating a paramagnetic phase. With a decrease in temperature, the magnetic order parameter increases gradually, indicating the transformation from the paramagnetic to a ferromagnetic phase around 350 K. Thus, the magnetic transition temperature (T_c^A) in the austenite phase also matches very well with the experimental value. With a further decrease in temperature, near the T_M, a small

kink, indicating a weak magnetoelastic coupling, is observed in the magnetic order parameter (m). With an applied external magnetic field of 5 T, T_M decreases, and the T_c^A increases in agreement with the experimental trend.

The calculated magnetic specific heat (C_{mag}) [Eq. (10)] is shown in Fig. 6(b). The total specific heat is also calculated as a function of temperature by calculating the lattice specific heat (C_{lat}) [Eq. (12)]. In the absence of experimental result on this compound, the Debye temperature Θ_D was taken as 222 K, the experimental Θ_D of Ni_2MnSb [72]. Here we assumed that the lattice specific heat does not contribute significantly to the isothermal entropy change, i.e., there is no significant impact of the application of magnetic field on C_{lat}. The isothermal entropy change, from lattice contributions across the magnetostructural transition, is not significant as long as the Debye temperature does not depend strongly on the magnetization and magnetic field. Two peaks can be observed in the specific heat curves, one at higher temperature corresponds to the second-order magnetic transition from paramagnetic to ferromagnetic phase, while the other at lower temperature corresponds to the structural transformation from austenite to martensite phases.

The magnetic entropy curve [in Fig. 6(d)] has been obtained by integrating the magnetic specific heat curves using Eq. (11) both at zero field and a field of 5 T. At very low temperatures, the calculated entropy has lower values, as expected, and increases with an increase in temperature, saturating at high temperatures beyond the magnetic transformation in the austenite phase. Upon application of the external magnetic field, the entropy of the system decreases as the system undergoes the magnetic transformation, while the entropy increases at the structural transformation. The insets of Fig. 6(d) show the changes in the entropy of the system
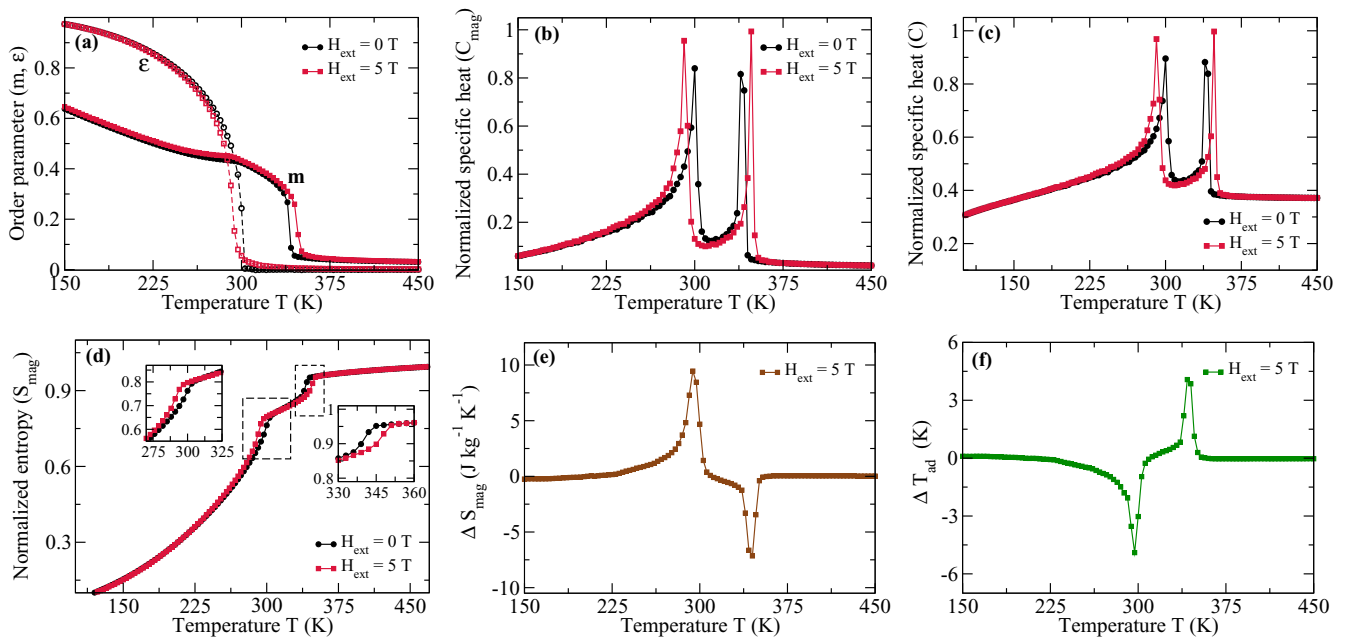

FIG. 6. The calculated temperature dependence of (a) magnetic (m) and strain (ε) order parameters, (b) and (c) normalized magnetic and total specific heat (C_{mag} and C, respectively), (d) normalized magnetic entropy (S_{mag}) in an external field of 0 and 5 T, and the temperature dependence of (e) the isothermal magnetic entropy change (ΔS_{mag}) and (f) adiabatic temperature change (ΔT_{ad}) due to change in the magnetic field from 0 to 5 T are shown. The results are for $Ni_{2-x}(Fe/Co)_xMn_{1+z-y}Cu_ySb_{1-z}$, with $z = 0.52$, $x = 0.00$, $y = 0.00$.
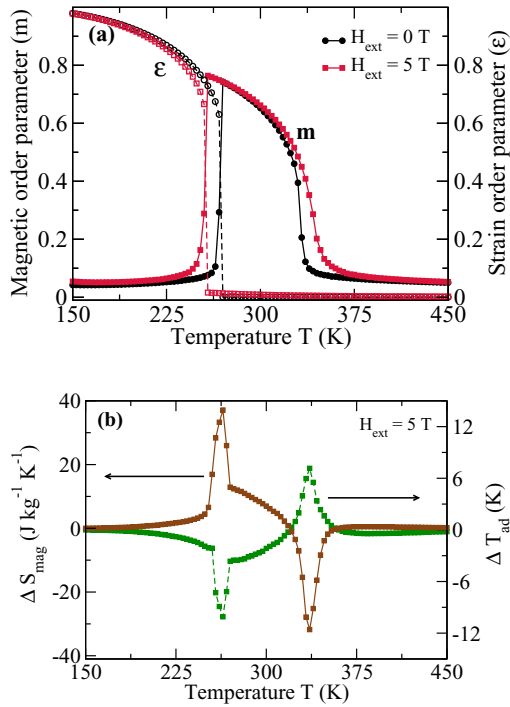
FIG. 7. The calculated temperature dependence of (a) magnetic (m) and strain (ε) order parameter in an external field of 0 and 5 T and (b) the isothermal magnetic entropy change (ΔS_{mag}) and adiabatic temperature change (ΔT_{ad}) due to change in the magnetic field from 0 to 5 T in Ni$_{2-x}$Co$_x$Mn$_{1+z-y}$Cu$_y$Sb$_{1-z}$; $z = 0.52$, $x = 0.20$, $y = 0.00$.
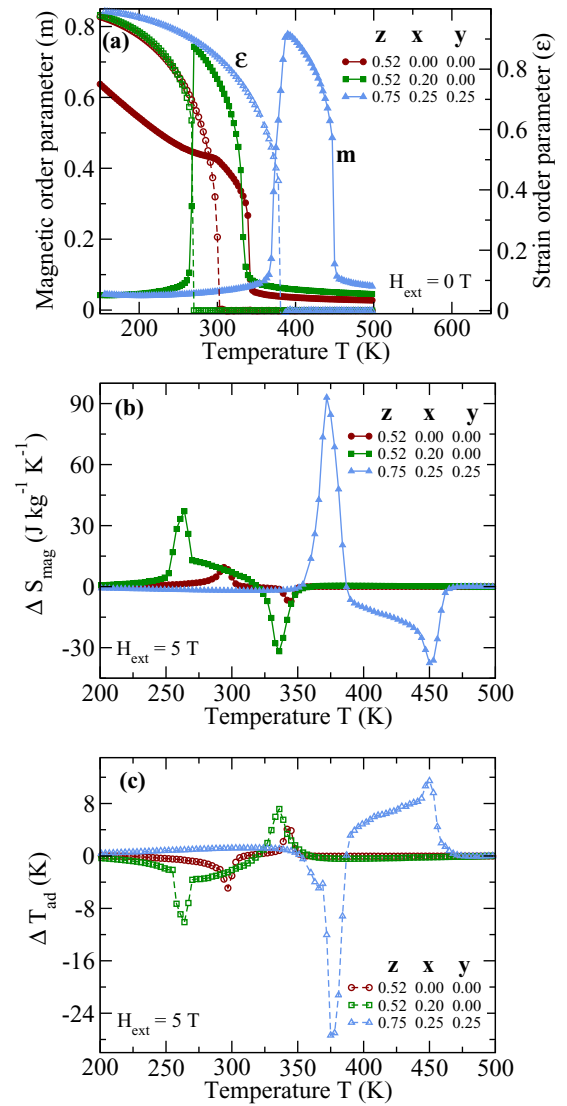

FIG. 8. The calculated temperature dependence of (a) magnetic (m) and strain (ε) order parameter in the absence of an external field, (b) the isothermal magnetic entropy change (ΔS_{mag}), and (c) adiabatic temperature change (ΔT_{ad}) due to change in the magnetic field from 0 to 5 T in Ni$_{2-x}$Co$_x$Mn$_{1+z-y}$Cu$_y$Sb$_{1-z}$; $z = 0.75$, $x = 0.25$, $y = 0.25$. Results for the reference compositions Ni$_2$Mn$_{1.52}$Sb$_{0.48}$ and Ni$_{1.8}$Co$_{0.2}$Mn$_{1.52}$Sb$_{0.48}$ have also been included for comparison.

when the structural (inset with lower temperature range) and magnetic (inset with higher temperature range) transformations take place.

The magnetic field induced isothermal entropy change ΔS_{mag} [Eq. (13)] and the adiabatic temperature change ΔT_{ad} [Eq. (14)] are shown in Figs. 6(e) and 6(f), respectively. The maximum change in entropy is positive for structural transformation and negative for the magnetic transformation. Hence, we have an inverse magnetocaloric effect (cooling of the material in the presence of magnetic field) during structural transformation, while regular magnetocaloric effect (heating of the material in the presence of magnetic field) as the magnetic transformation takes place. A maximum value of isothermal entropy change of 9.8 J kg^{-1} K^{-1} is obtained at the first-order magnetostructural transition, in good agreement with the experimental observation [22,23]. Our calculations predict a large value of nearly 5 K of ΔT_{ad} which, however, could not be compared with experiments due to the unavailability.

We next applied the same formalism to the Co substituted compound Ni$_{1.8}$Co$_{0.2}$Mn$_{1.52}$Sb$_{0.48}$. Due to the availability of experimental results [23], we could make a direct comparison. The results are shown in Fig. 7. The *ab initio* magnetic exchange parameters used here are shown in Figs. 1(c) and 1(d), Ref. [56]. In here, the number of spin states for Co was taken to be $q_{Co} = 4$. The parameters in the Hamiltonian were adjusted, such that the experimental value of T_M ($\approx$260 K) and T_c^A ($\approx$330 K) could be reproduced. This is evident from the curves of m and ε in Fig. 7(a).

The parameters used for this calculation are listed in Table II. The directions of shifts in T_M and T_c^A under application of an external magnetic field of 5 T are in agreement with the experimental trends. One noteworthy point is that in contrast to the Ni$_2$Mn$_{1.52}$Sb$_{0.48}$, magnetization changes sharply at the structural transition in this case. This is important to obtain a giant MCE. This significant change in magnetization can be understood by analyzing the magnetic exchange interactions between different atom pairs in both structural phases (Figs. 1(c) and 1(d), Ref. [56]). While for both Ni$_2$Mn$_{1.52}$Sb$_{0.48}$ and Ni$_{1.8}$Co$_{0.2}$Mn$_{1.52}$Sb$_{0.48}$, the dominant antiferromagnetic interaction between Mn atoms are four times larger in the tetragonal phase, in comparison to

that in the austenite phase, larger ferromagnetic interactions due to the Mn1(Mn2)-Co atom pairs in the austenite phase appears for the later compound. This can be correlated to the larger change in the magnetization for Co substituted compound. The MCE quantities ΔS_{mag} and ΔT_{ad}, calculated as a function of temperature, as shown in Fig. 7(b) and the maximum ΔS_{mag} of nearly 40 J kg^{-1} K^{-1}, much larger than the Ni$_2$Mn$_{1.52}$Sb$_{0.48}$, is obtained due to the magnetostructural transition near T_M in an applied field of 5 T. This is in excellent agreement with the experimental value [23] of 35 J kg^{-1} K^{-1}. We also obtained a large value of ΔT_{ad} that could not be verified in the absence of experimental results.

The excellent agreement of the results obtained for the two compounds with the experimental observations validates the approach adopted here for computing the variables quantifying MCE. Therefore, we apply the same formalism for the cosubstituted compound Ni$_{1.75}$Co$_{0.25}$Mn$_{1.50}$Cu$_{0.25}$Sb$_{0.25}$. The results are presented in Fig. 8. The *ab initio* calculated exchange interactions used are shown in Figs. 1(e) and 1(f), Ref. [56]. The values of elastic and magnetoelastic parameters were tuned (Table II) to fix the T_M at 398 K, as predicted in Sec. III D, and T_c^A at 460 K as calculated through MCS in Table I. For the purpose of comparison, we have included the results for Ni$_2$Mn$_{1.52}$Sb$_{0.48}$ and Ni$_{1.8}$Co$_{0.2}$Mn$_{1.52}$Sb$_{0.48}$. We find that cosubstitution leads to an increase in the working temperature (T_M). Also, the change in magnetization near MPT is larger [Fig. 8(a)]. Both these characteristics were desired for a larger MCE in cosubstituted compounds. The calculated MCE quantities [Figs. 8(b) and 8(c)] meet this expectation. The results demonstrate that ΔS_{mag}, four times higher than Ni$_2$Mn$_{1.52}$Sb$_{0.48}$ and two times higher than Ni$_{1.8}$Co$_{0.2}$Mn$_{1.52}$Sb$_{0.48}$, are obtained. Stronger ferromagnetic interactions in the austenite phase of cosubstituted compound (Figs. 1(e) and 1(f), Ref. [56]), in comparison with the other two compounds, can be correlated to this amplified effect.

IV. CONCLUSIONS

Using first-principles electronic structure calculations, we provide a protocol to systematically screen materials, potential to exhibit giant MCE driven by a first-order magnetostructural transition at temperatures near room temperature or above, among given Heusler family of compounds. We apply this approach to find target compounds in the cosubstituted Ni-Mn-Sb family; the cosubstitution done at Ni and Mn sites. Our approach predicted four new compounds in the two cosubstituted families. In order to validate our predictions, we took recourse to a thermodynamic model to compute the MCE properties in one of these predicted compounds. The robustness and accuracy of the computational approach using the thermodynamic model that takes into account magnetic, elastic, and magnetoelastic effects in equal footing, is demonstrated by computing the MCE parameters in Ni$_2$Mn$_{1.52}$Sb$_{0.48}$ and Co substituted Ni$_{1.8}$Co$_{0.2}$Mn$_{1.52}$Sb$_{0.48}$ compounds where experimental results are available. Further computation of MCE parameters for one of the predicted compounds yields magnetic entropy change as large as four times in comparison to that observed experimentally. Thus, this established the protocol for screening materials from a large database adopted in this work. This work, apart from demonstrating the power of *ab initio* based approaches for computations of MCE parameters, offers experimentalists a broader scope to explore new materials where giant MCE, driven by first-order magnetoelastic transition, can be realized through cosubstitution in Heusler compounds.

[1] L. P. Oliva, Pace Envtl. L. Rev. **7**, 213 (1989).

[2] T. Tegusi, Thesis, Universiteit van Amsterdam, 2003.

[3] J. Banks, 2002 Report of the Methyl Bromide Technical Options Committee, UNEP (2002).

[4] I. Hughes, M. Däne, A. Ernst, W. Hergert, M. Lüders, J. Poulter, J. Staunton, A. Svane, Z. Szotek, and W. Temmerman, Nature (London) **446**, 650 (2007).

[5] V. K. Pecharsky and K. A. Gschneidner Jr., Phys. Rev. Lett. **78**, 4494 (1997).

[6] V. K. Pecharsky and K. A. Gschneidner, Jr., Adv. Mater. **13**, 683 (2001).

[7] A. M. Tishin and Y. I. Spichkin, *The Magnetocaloric Effect and Its Applications* (CRC, Boca Raton, FL, 2016).

[8] A. De Campos, D. L. Rocco, A. M. G. Carvalho, L. Caron, A. A. Coelho, S. Gama, L. M. Da Silva, F. C. Gandra, A. O. Dos Santos, L. P. Cardoso *et al.*, Nat. Mater. **5**, 802 (2006).

[9] S. Fujieda, A. Fujita, and K. Fukamichi, Appl. Phys. Lett. **81**, 1276 (2002).

[10] H. Wada and Y. Tanabe, Appl. Phys. Lett. **79**, 3302 (2001).

[11] O. Tegus, E. Brück, and L. Zhang, Physica B **319**, 174 (2002).

[12] Z. Li, J. L. Sánchez Llamazares, C. F. Sánchez-Valdés, Y. Zhang, C. Esling, X. Zhao, and L. Zuo, Appl. Phys. Lett. **100**, 174102 (2012).

[13] Z. Li, Y. Zhang, C. F. Sánchez-Valdés, J. L. Sánchez Llamazares, C. Esling, X. Zhao, and L. Zuo, Appl. Phys. Lett. **104**, 044101 (2014).

[14] T. Krenke, M. Acet, E. F. Wassermann, X. Moya, L. Mañosa, and A. Planes, Phys. Rev. B **72**, 014412 (2005).

[15] T. Krenke, E. Duman, M. Acet, E. F. Wassermann, X. Moya, L. Mañosa, A. Planes, E. Suard, and B. Ouladdiaf, Phys. Rev. B **75**, 104414 (2007).

[16] M. Pasquale, C. P. Sasso, L. H. Lewis, L. Giudici, T. Lograsso, and D. Schlagel, Phys. Rev. B **72**, 094435 (2005).

[17] A. K. Pathak, M. Khan, I. Dubenko, S. Stadler, and N. Ali, Appl. Phys. Lett. **90**, 262504 (2007).

[18] T. Krenke, E. Duman, M. Acet, E. F. Wassermann, X. Moya, L. Mañosa, and A. Planes, Nat. Mater. **4**, 450 (2005).

[19] S. E. Muthu, N. R. Rao, M. M. Raja, D. R. Kumar, D. M. Radheep, and S. Arumugam, J. Phys. D **43**, 425002 (2010).

[20] D. Cong, L. Huang, V. Hardy, D. Bourgault, X. Sun, Z. Nie, M. Wang, Y. Ren, P. Entel, and Y. Wang, Acta Mater. **146**, 142 (2018).

[21] N. Duc, T. Thanh, N. Yen, P. Thanh, N. Dan, and T. Phan, J. Korean Phys. Soc. **60**, 454 (2012).

[22] M. Khan, N. Ali, and S. Stadler, J. Appl. Phys. **101**, 053919 (2007).

[23] A. K. Nayak, K. Suresh, and A. Nigam, J. Phys. D **42**, 035009 (2009).

[24] A. K. Nayak, K. Suresh, and A. Nigam, J. Phys. D **42**, 115004 (2009).

[25] Z. Han, D. Wang, C. Zhang, H. Xuan, J. Zhang, B. Gu, and Y. Du, J. Appl. Phys. **104**, 053906 (2008).

[26] R. Sahoo, A. K. Nayak, K. Suresh, and A. Nigam, J. Appl. Phys. **109**, 123904 (2011).

[27] M. Zelený, A. Sozinov, L. Straka, T. Björkman, and R. M. Nieminen, Phys. Rev. B **89**, 184103 (2014).

[28] V. V. Sokolovskiy, P. Entel, V. Buchelnikov, and M. Gruner, Phys. Rev. B **91**, 220409(R) (2015).

[29] A. Perez-Checa, J. Feuchtwanger, J. Barandiaran, A. Sozinov, K. Ullakko, and V. Chernenko, Scr. Mater. **154**, 131 (2018).

[30] S. Ghosh and S. Ghosh, Phys. Rev. Mater. **4**, 025401 (2020).

[31] J. Amaral, N. Silva, and V. Amaral, Appl. Phys. Lett. **91**, 172503 (2007).

[32] P. Álvarez, P. Gorria, and J. Blanco, Phys. Rev. B **84**, 024412 (2011).

[33] K. Szałowski, T. Balcerzak, and A. Bobák, J. Magn. Magn. Mater. **323**, 2095 (2011).

[34] C. Triguero, M. Porta, and A. Planes, Phys. Rev. B **73**, 054401 (2006).

[35] E. Nobrega, N. de Oliveira, P. Von Ranke, and A. Troper, J. Phys.: Condens. Matter **18**, 1275 (2006).

[36] V. D. Buchelnikov, V. Sokolovskiy, S. Taskaev, and P. Entel, *Materials Science Forum* (Trans Tech Publ, Baech, Switzerland, 2010), Vol. 635, pp. 137–142.

[37] V. Buchelnikov, V. Sokolovskiy, S. Taskaev, V. Khovaylo, A. Aliev, L. Khanov, A. Batdalov, P. Entel, H. Miki, and T. Takagi, J. Phys. D **44**, 064012 (2011).

[38] V. D. Buchelnikov, V. V. Sokolovskiy, H. C. Herper, H. Ebert, M. E. Gruner, S. V. Taskaev, V. V. Khovaylo, A. Hucht, A. Dannenberg, M. Ogura *et al.*, Phys. Rev. B **81**, 094411 (2010).

[39] E. Nóbrega, N. de Oliveira, P. von Ranke, and A. Troper, Phys. Rev. B **72**, 134426 (2005).

[40] N. Singh and R. Arróyave, J. Appl. Phys. **113**, 183904 (2013).

[41] V. Sokolovskiy, V. Buchelnikov, S. Taskaev, V. Khovaylo, M. Ogura, and P. Entel, J. Phys. D **46**, 305003 (2013).

[42] V. Sokolovskiy, V. Buchelnikov, K. Skokov, O. Gutfleisch, D. Karpenkov, Y. Koshkid'ko, H. Miki, I. Dubenko, N. Ali, S. Stadler *et al.*, J. Appl. Phys. **114**, 183913 (2013).

[43] V. Sokolovskiy, M. Zagrebin, and V. D. Buchelnikov, J. Magn. Magn. Mater. **459**, 295 (2018).

[44] V. Sokolovskiy, O. Miroshkina, M. Zagrebin, and V. Buchelnikov, J. Appl. Phys. **127**, 163901 (2020).

[45] P. E. Blöchl, Phys. Rev. B **50**, 17953 (1994).

[46] G. Kresse and D. Joubert, Phys. Rev. B **59**, 1758 (1999).

[47] G. Kresse and J. Furthmüller, Phys. Rev. B **54**, 11169 (1996).

[48] J. P. Perdew, K. Burke, and M. Ernzerhof, Phys. Rev. Lett. **77**, 3865 (1996).

[49] H. Ebert, D. Koedderitzsch, and J. Minar, Rep. Prog. Phys. **74**, 096501 (2011).

[50] A. I. Liechtenstein, M. Katsnelson, V. Antropov, and V. Gubanov, J. Magn. Magn. Mater. **67**, 65 (1987).

[51] V. Sokolovskiy, V. Buchelnikov, M. Zagrebin, P. Entel, S. Sahoo, and M. Ogura, Phys. Rev. B **86**, 134418 (2012).

[52] M. Meinert, J.-M. Schmalhorst, and G. Reiss, J. Phys.: Condens. Matter **23**, 036001 (2010).

[53] D. P. Landau and K. Binder, *A Guide to Monte Carlo Simulations in Statistical Physics* (Cambridge University Press, Cambridge, 2014).

[54] M. Zagrebin, V. Sokolovskiy, and V. Buchelnikov, J. Phys. D **49**, 355004 (2016).

[55] A. Kundu, S. Ghosh, and S. Ghosh, Phys. Rev. B **96**, 174107 (2017).

[56] See Supplemental Material at http://link.aps.org/supplemental/10.1103/PhysRevB.103.054101 for detailed discussions on computational methods to calculate Curie temperature in austenite phase, the results on structural and magnetic properties for single Fe, Co, and Cu substituted systems, and magnetic exchange parameters both in austenite and martensite phases.

[57] N. Singh, E. Dogan, I. Karaman, and R. Arróyave, Phys. Rev. B **84**, 184201 (2011).

[58] M. Blume, V. Emery, and R. B. Griffiths, Phys. Rev. A **4**, 1071 (1971).

[59] E. Vives, T. Castán, and P.-A. Lindgård, Phys. Rev. B **53**, 8915 (1996).

[60] M. Newman and G. Barkema, *Monte Carlo Methods in Statistical Physics* (Oxford University Press, New York, 1999), Chaps. 1–4.

[61] X. Moya, D. González-Alonso, L. Mañosa, A. Planes, V. Garlea, T. A. Lograsso, D. L. Schlagel, J. L. Zarestky, S. Aksoy, and M. Acet, Phys. Rev. B **79**, 214118 (2009).

[62] S. Ghosh and S. Ghosh, Phys. Rev. B **101**, 024109 (2020).

[63] A. Ghosh and K. Mandal, Appl. Phys. Lett. **104**, 031905 (2014).

[64] V. Sánchez-Alarcos, V. Recarte, J. Pérez-Landazábal, and G. Cuello, Acta Mater. **55**, 3883 (2007).

[65] S. Ghosh and S. Ghosh, Phys. Rev. B **99**, 064112 (2019).

[66] C.-M. Li, H.-B. Luo, Q.-M. Hu, R. Yang, B. Johansson, and L. Vitos, Phys. Rev. B **84**, 024206 (2011).

[67] A. Chakrabarti, M. Siewert, T. Roy, K. Mondal, A. Banerjee, M. E. Gruner, and P. Entel, Phys. Rev. B **88**, 174116 (2013).

[68] V. Sokolovskiy, M. Zagrebin, and V. Buchelnikov, J. Phys. D **50**, 195001 (2017).

[69] J. Du, Q. Zheng, W. J. Ren, W. J. Feng, X. G. Liu, and Z. D. Zhang, J. Phys. D **40**, 5523 (2007).

[70] M. Khan, I. Dubenko, S. Stadler, and N. Ali, J. Phys.: Condens. Matter **20**, 235204 (2008).

[71] R. Sahoo, K. Suresh, and A. Das, J. Magn. Magn. Mater. **371**, 94 (2014).

[72] S. Podgornykh, S. Streltsov, V. Kazantsev, and E. Shreder, J. Magn. Magn. Mater. **311**, 530 (2007).